Design and Implementation of a Lightweight Bioinspired Pectoral Fin Driven by SMA

Shiwu Zhang, Bo Liu, Lei Wang, Qin Yan, Kin Huat Low, and Jie Yang

***Abstract*—Pectoral fins play an important role in the fish swimming performance, especially in maneuverability underwater. This paper presents the swimming propulsion by means of a flexible and lightweight pectoral fin inspired by a Koi Carp. The fin is driven by embedded shape memory alloy (SMA) wires. In this paper, the kinematics of a pectoral fin from a live Koi Carp fish is first studied. The motion of fin rays is analyzed, in which four basic patterns are extracted from the motion of the pectoral fin captured experimentally, especially the motion in retreating and hovering. Inspired by the fin motion of the live fish, an SMA-driven fin ray providing a two-degree-of-freedom bending motion is proposed. The detailed design of the bioinspired pectoral fin driven by SMA-driven rays is then presented. The basic unit is an SMA-driven plate with two SMA wires embedded on the two opposite sides of a plastic plate. The SMA-driven plate can bend by a pulse width modulation current delivered through SMA wires. An assembled SMA fin ray is next formed by two SMA plates, which are placed in series with their cross sections perpendicular to each other. As a result, a lightweight bioinspired pectoral fin is constructed by placing radially multiple SMA fin rays. The integrated pectoral fin is able to exhibit four patterns extracted in the biological kinematic study. The simulation and experimental optimization on the SMA-driven plate are presented in the final part of this paper. The diameter of SMA wires is optimized and the oscillation angle of SMA plate is obtained. The experiment is also conducted to evaluate the motions of the bioinspired pectoral fin. The result demonstrates that the SMA-based fin is effective in driving the bioinspired fin. Moreover, the bioinspired pectoral fin is able to perform complex motions that can contribute to the maneuverability of fish robots.**

***Index Terms*—Bioinspired pectoral fin, fin patterns, maneuverability, shape memory alloy (SMA), SMA-driven plate.**

I. Introduction

FISHES have attracted the attention of scientists over several decades for their excellent swimming performance. They can swim with a high efficiency and good maneuverability in turning, hovering, retreating, and braking [1]–[4]. Fish's fins play an important role in fish swimming, and they are vital for thrust generating, balance keeping, maneuverability, etc. For example, according to the two classifications of the fish propulsion: body and caudal fin (BCF) mode and median and/or paired fin (MPF) mode, the caudal fin in the BCF mode is the main propeller, while pectoral fins maneuver with other fins. For rajiform and labriform in the MPF mode, the pectoral fins act as the thrust generation [2]. Researchers have conducted physiology, morphology, and kinematic studies on pectoral fins that vary from fish to fish. Westneat *et al.* [5], [6] studied the pectoral fin of labriform swimmers, in which 3-D kinematic data of the pectoral fin were presented. Thorsen and Westneat [7] investigated the detailed musculoskeletal structure of the pectoral fins associated with 12 species of labriform propulsion. Rosenberger [8], [9] studied the morphology of the stingray pectoral fin. He also described the general swimming behavior of the pectoral fin locomotion of eight species of batoids. Lauder *et al.* [10]–[12] studied the complex 3-D surface movement of the bluegill sunfish pectoral fin in the aspects of anatomy, morphology, and kinematics.

Inspired by the structure and kinematic of various pectoral fins, researchers have developed a variety of biorobotic pectoral fins. Sitorus *et al.* [13] designed a paired pectoral fins based on a labriform fish. Yang *et al.* [14] developed oscillating pectoral fins to drive a robotic fish inspired by cownose ray. Low *et al.* [15]–[17] designed an undulation device to mimic the pectoral fin of stingrays in rajiform swimmers. However, most of these bioinspired pectoral fins are rigid and are capable of simple motions only. As noted in the study on pectoral fins of the sunfish [10]–[12], the flexible structure and 3-D motions of the pectoral fin greatly affect its performance. In this connection, Tangorra *et al.* [18]–[20] developed a flexible robotic pectoral fin based on the bluegill sunfish. The team studied the highly deformable fish fin's effect on the propulsive force. However, the servomotors, tendons, and hinges are formed to actuate the robotic fin. This leads to a bulky and relatively heavy robotic fish body.

In order to imitate the complex motions of pectoral fins with simple and lightweight structure at the same time, smart materials are adopted. Smart materials such as ionic conducting polymer film [21], shape memory alloy (SMA) [22]–[24], ionic polymer metal composite [25]–[28] have been adopted in biomimetic underwater robots. Wang *et al.* [29], [30] developed an SMA-driven caudal fin and achieved a high locomotion performance of a robotic squid. In fact, SMA has several advantages that are suitable for an biomimetic device [31]–[33]: 1) SMA is

Manuscript received February 4, 2013; revised September 5, 2013; accepted October 30, 2013. Date of publication January 2, 2014; date of current version June 13, 2014. Recommended by Technical Editor A. Menciassi. This work was supported in part by the National Natural Science Foundation of China under Grant 50975270 and in part by the Fundamental Research Funds for the Central Universities of China (WK2090090002).

S. Zhang, B. Liu, L. Wang, and J. Yang are with the Department of Precision Machinery and Instrumentation, University of Science and Technology of China, Hefei 230026, China (e-mail: swzhang@ustc.edu.cn; yunjue@mail.ustc.edu.cn; lwang020@mail.ustc.edu.cn; jieyang@ustc.edu.cn).

Q. Yan is with Suzhou University of Science and Technology, Suzhou 215011, China (e-mail: yanqin@mail.ustc.edu.cn).

K. H. Low is with the School of Mechanical and Aerospace Engineering, Nanyang Technological University, Singapore 639798 (e-mail: mkhlow@ntu.edu.sg).

Color versions of one or more of the figures in this paper are available online at http://ieeexplore.ieee.org.

Digital Object Identifier 10.1109/TMECH.2013.2294797

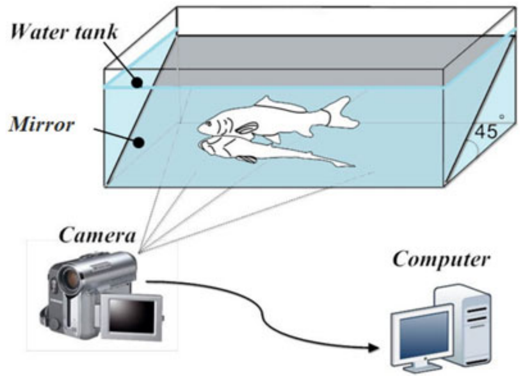

Fig. 1. Sketch of the kinematic experimental setup.

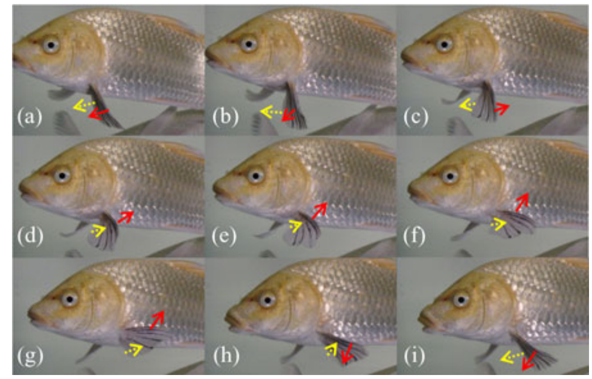

Fig. 2. Motion cycle of the pectoral fin in fish retreating. Solid arrows represent the motion direction of the dorsal leading ray, and dashed arrows represent the motion direction of the ventral leading ray. The time interval of two neighboring pictures is 50 ms. Note that the view of the pectoral fin in the mirror is excluded in the present figure, for clarity.

the integration of the driver and structure, which simplifies the device largely; 2) SMA can generate a notable strain (up to 8%) and a significant stress (up to 600 MPa) under a relative low voltage; 3) SMA's actuated frequency underwater (up to 2 Hz) is appropriate. Therefore, we adopt SMA as the actuator of a lightweight bioinspired pectoral fin, which can exhibit complex shape and motions [34]–[36].

The remaining of this paper is organized as follows. The kinematics of the pectoral fin from a Koi Carp is first investigated and described. Four basic patterns of the pectoral fin during fish hovering and retreating are extracted in Section II. The detailed design of the flexible bioinspired pectoral fin capable of complex motions actuated by SMA is presented in Section III. The simulation in thermodynamics and the experimental optimization on the SMA plates are conducted and discussed in Section IV. In Section V, the hydrodynamic experiment on the bioinspired fin is conducted. The force in the flapping and undulation is presented and analyzed. In Section VI, the advantages of the developed bioinspired fin are discussed. The comparison between our bioinspired fin and other robotic fins is also presented. Finally, concluding remarks are provided in Section VI.

II. Kinematics Study of Biological Pectoral Fins

Koi Carp possesses excellent swimming performance by the coordinated motions of pectoral fins and other fins. The kinematics study on pectoral fins of a Koi Carp was conducted with a high-speed camera. The image resolution is 2816 × 2112 pixels, and the photograph speed is 60 frame/s. A reflective mirror is placed in the water tank as shown in Fig. 1. By virtue of the mirror, we can obtain two views of the pectoral fin simultaneously with only one camera. Accordingly, continuous 3-D morphologies of the pectoral fin can be obtained with the multiview imaging system and digital imaging process [37].

By virtue of the motion study, we observed that as the Koi Carp hovers or retreats, pectoral fins move continuously while other fins (dorsal fin, ventral fin, anal fin, and caudal fin) remain nearly still. This implies that the pectoral fins play a vital role during retreating and hovering. However, when the fish steady swims or accelerates, the propulsion forces mainly come from the motion of the caudal fin, the pectoral fins only assist swimming. For the following discussion, we select two basic maneuvers to observe the motions of pectoral fins: retreating and hovering.

A. *Pectoral Fin in Retreating*

The motion of the pectoral fin during retreating is divided into two stages: in-stroke [see Fig. 2(c)–(g)] and out-stroke [see Fig. 2 (a) and (b), (h) and (i)]. The motion is a hybrid mode that combines paddling, rotating, expanding, and shrinking. During out-stroke, the pectoral fin expands in order to increase flapping area, thus increases retreating force. As for in-stroke, the fin surface reduces. The angle between the fin surface and the vertical plane decreases. And the propulsive force also decreases. The motion direction of ventral leading ray and dorsal leading ray is coincident throughout most of the motion cycle.

The frequency of the pectoral fin motion is about 2 Hz. Over the motion cycle, the duty ratio of out-stroke is about 40%, whereas the duty ratio of in-stroke is about 60%. The phenomenon of "fast out-stroke, slow in-stroke" reflects the asymmetry of motion.

B. *Pectoral Fin in Hovering*

During hovering, the motion of the fish body is almost still (see Fig. 3). A small lift provided by the small swing of pectoral fins maintains the body posture. There is an undulation and a small amplitude oscillation in the motion of the pectoral fin. The motion of the pectoral fin during hovering can also be divided into two stages: out-stroke [see Fig. 3(a), and (b), (g), (h), and (i)] and in-stroke [see Fig. 3(c)–(f)]. During out-stroke, the pectoral fin expands to increase flapping surface area. During in-stroke, the fin shrinks to reduce the flapping surface area.

The pectoral fin almost keeps vertical to the longitudinal axis of the body during hovering. The fin surface displays the state of bending, cupping, undulation, and their complex combination. The motion frequency of the pectoral fin is about 2 Hz.

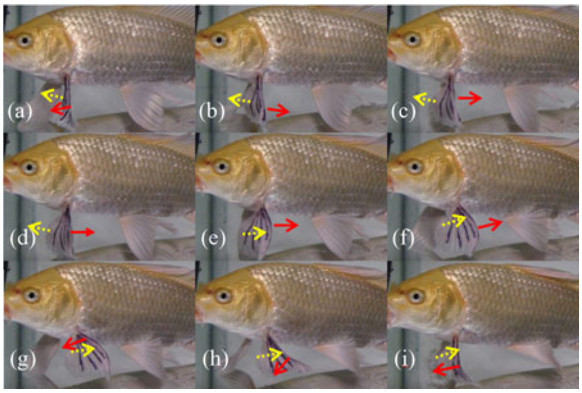

Fig. 3. Motion cycle of the pectoral fin during hovering. Solid arrows represent the motion direction of the dorsal leading ray, and dashed arrows represent the motion direction of the ventral leading ray. The time interval of neighboring pictures is 50 ms. Note that the view of the pectoral fin in the mirror is excluded in the figure, for clarity.

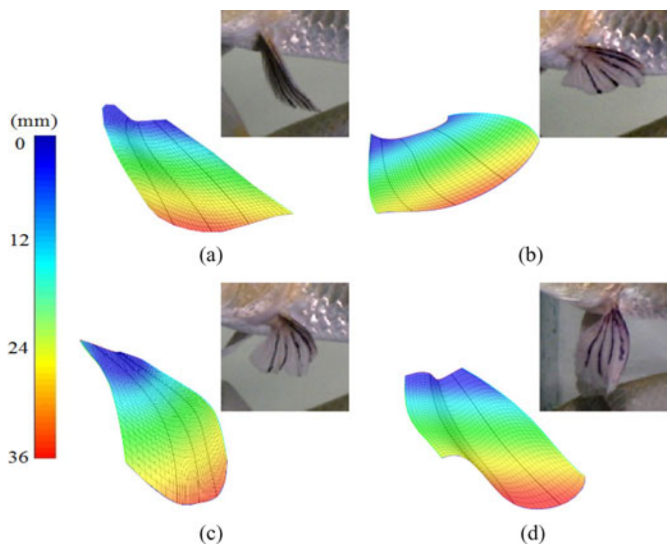

Fig. 4. Four basic patterns of the pectoral fin: (a) Relaxation [a relevant pectoral fin image can be obtained from Fig. 2(a)]. (b) Expansion [see Fig. 2(f)]. (c) Bending [see Fig. 2(e)]. (d) Undulation [see Fig. 3(e)]. The ranges from top to bottom reflect the distance from the pectoral fin base, top range (0–12) of areas implies fin parts is near the fin base, and bottom range (24–36) of areas denotes a reverse situation.

C. Basic Patterns and Motions of the Pectoral Fin

The pectoral fin displays complex 3-D shapes during fish retreating and hovering. Four basic patterns of the pectoral fin are observed and extracted through digital image processing on the captured images in experiments by the multiview imaging system: 1) relaxation: dorsal leading ray, ventral leading ray, and other rays are basically in the same plane. Meanwhile, the rays lie straight and are close to each other, as shown in Fig. 4(a); 2) expansion: dorsal leading ray and ventral leading ray expand span-wise with the fin surface area increasing, as shown in Fig. 4(b); 3) bending: fin rays bend into one direction, the fin surface displays a parabolic surface, as shown in Fig. 4(c); 4) undulation: there are phase differences in the motions of neighboring fin rays. The fin surface displays a "w" shape, as shown in Fig. 4(d).

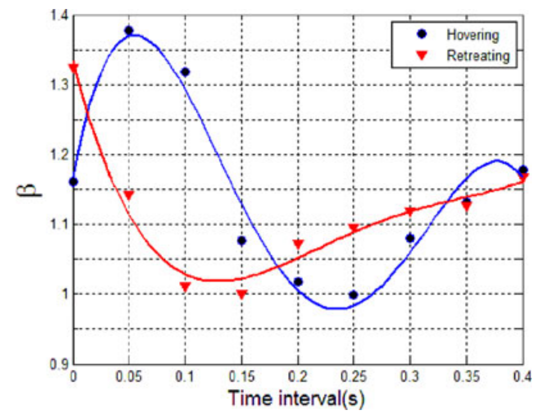

Fig. 5. Expansion coefficient β of the pectoral fin during retreating and hovering. The triangular points and dots are the expansion degree during retreating and hovering, respectively. The curve is obtained by fourth-order polynomial fitting. The standard deviation of the surface area during hovering is 0.03, and the standard deviation of surface areas during retreating is 0.02.

The complex motions of the pectoral fins are categorized in three movement groups based on the four basic patterns, 1) motions within the pattern. For example, undulation motion denotes fin undulating with certain wave number and wave speed, flapping motion denotes fin alternately bending into opposite directions; 2) transformations between the patterns, such as expanding and shrinking between relaxation and expansion; 3) combination of various basic patterns, for example, undulation with the fin expansion. The four associated patterns of pectoral fin provide the reference and foundation for the design and the control of the bioinspired flexible pectoral fin.

The surface area of the pectoral fin during retreating and hovering is also extracted by digital image processing. An expansion coefficient β is introduced to describe the area change in a fin motion cycle with the expression of $\beta = S/S_0$, in which S_0 denotes the minimum surface area during retreating and hovering, while S denotes the current surface area. Fig. 5 shows the expansion degree of the pectoral fin during hovering and retreating, respectively. The maximum expansion coefficient during retreating is 1.33, whereas it is about 1.4 during hovering.

D. Motions of Fin Rays

From the images captured by the multi-view imaging system, we are able to extract spatial positions of the fin rays with the digital imaging process. We found in the experiment that: 1) the base of the fin rays nearly keep fixed to the fish body, 2) there are two degrees of freedom (DoF) for each fin ray in a fin beat, which has also been verified by the study on the pectoral fin of the sunfish [12], [38], in which two pairs of muscles control a fin ray to achieve a two-DoF bending motion.

Fig. 6 shows the coordination of the fin rays of the Koi Carp during a fin beat, together with the fin angles. Fig. 7 shows the two angles of dorsal leading ray during fish retreating and hovering. The figures show that the fin ray performs the motion with two rotations.

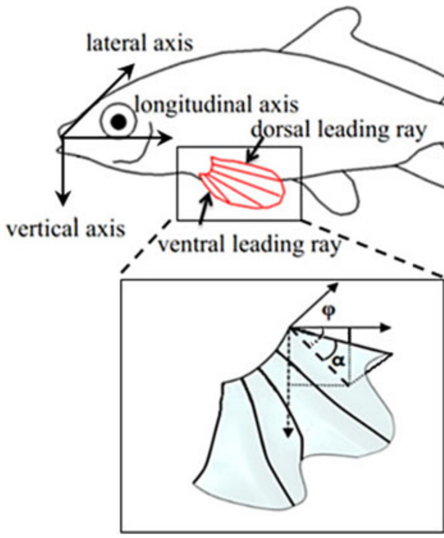

Fig. 6. Sketch of the coordinates of the Koi Carp and orientation of a fin ray in a fin beat. In the enlarged fin diagram, α stands for the angle between the root of the fin ray and the screen plane, while φ stands for the angle between the projection of the root of the fin ray in the screen plane and the longitudinal axis.

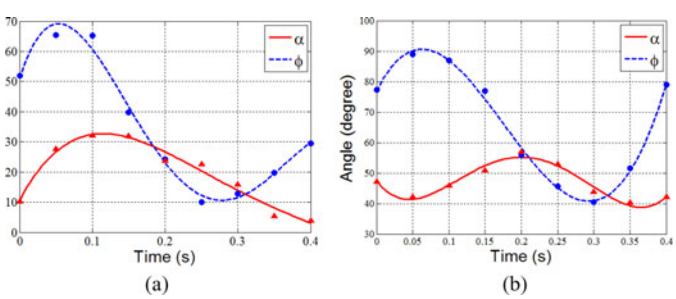

Fig. 7. Motions of the dorsal leading ray: (a) during retreating, the maximum angle changing is about 60° and (b) during hovering, the maximum angle changing is about 50°.

With the fin ray's dual rotations, the shape and the area of the pectoral fin changes continuously in a fin beat. The complex motions and shape changes of the pectoral fin come from the coordinated motions of the fin rays and the effect of the hydrodynamics. Therefore, the key factor to develop a bioinspired pectoral fin with complex motions is to design and control a fin ray that can deflect in two orthogonal directions.

The kinematics study provides us a deeper understanding on the motion of biological pectoral fins during retreating and hovering, which inspires the design and experiment of a lightweight bioinspired pectoral fin. First, the ray's two-DoFs bending motion provides a reference for the design of a bioinspired fin ray. Second, the four basic patterns of the pectoral fin provide the foundation for the design and the control of the bioinspired flexible pectoral fin. The design of a bioinspired pectoral fin is presented in the following section.

III. Design of a Lightweight Bioinspired Pectoral Fin

In our design of bioinspired pectoral fin, two mechanisms of SMA fin ray are compared according to the requirements

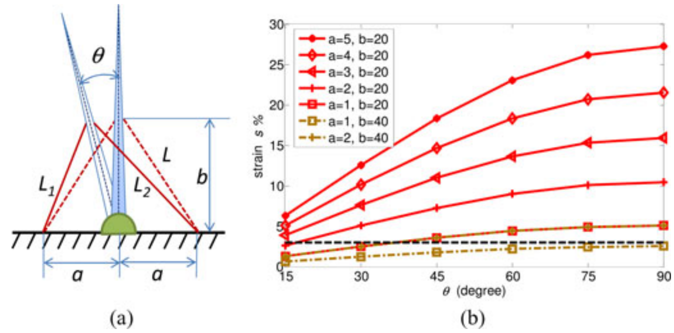

Fig. 8. Structure of the SMA fin ray: (a) fin ray with a hinge on its root, pulled by SMA wires (L_1 and L_2), where a denotes the distance from the fixed point of the SMA wire on base part to the root of the fin ray, and b denotes the distance from the fixed point of the SMA wire on the fin ray to the root of the fin ray; and (b) relationship of the deflection angle and strain of SMA wires (the dashed horizontal line denotes 3% strain). Note that θ denotes the angle that the fin ray deflects, and s denotes the strain that the SMA wire contracts.

obtained from the previous section. An SMA-driven plate that can achieve 1-D oscillation is next developed. An SMA fin ray that can execute a two-DoFs oscillation through SMA-driven plates is also presented. Finally, a flexible bioinspired pectoral fin that can perform basic patterns is produced.

A. *Selection of SMA Fin Ray Structures*

According to the characteristics of SMA and the kinematics of a biological fin ray, there are several constraints or requirements for the design of an SMA fin ray: 1) An SMA wire is able to provide a large recovery strains (3%) under a significant stress (about 300 MPa) with a long life (>1000 cycles), which have been verified by our experiments on SMA wires. An SMA spring may provide a much larger strain, if compared with that of an SMA wire. However, its large diameter and small recovery stress limit its application in a bioinspired underwater fin ray; 2) Each SMA fin ray can bend into two directions: the bending angle is relatively large (up to 60°); and the motion frequency is about 2 Hz.

From the biomimetic viewpoint, the SMA fin ray should adopt the structure that is shown in Fig. 8(a). In the figure, the fin ray is composed of a plastic stick with the radius getting smaller from the root to the tip. Two SMA wires, fixed between the fin ray and the base part, are the muscles to actuate the fin ray. If left SMA wire is heated to its austenitic starting temperature A_s, it will contract and pull the fin ray to deflect. While heating right SMA wire will lead the fin ray to deflect into the opposite direction. If we fix two more SMA wires on the fin ray and pull the fin ray deflected in the plane that is orthogonal to the screen, the bio-inspired fin ray will fulfill a two-DoF motion as a real fin ray does [12], [38]. However, the structure requires a large strain for SMA wires. We could obtain from Fig. 8 that the relationship between strain s and deflection angle θ as given by

$$s = \frac{L - L_1}{L} = 1 - \sqrt{a^2 + b^2 - 2ab\cos(\pi/2 - \theta)}/\sqrt{a^2 + b^2}. \tag{1}$$

The result of the relationship is depicted in Fig. 8(b). Some findings can be concluded from the figure: 1) it is difficult for

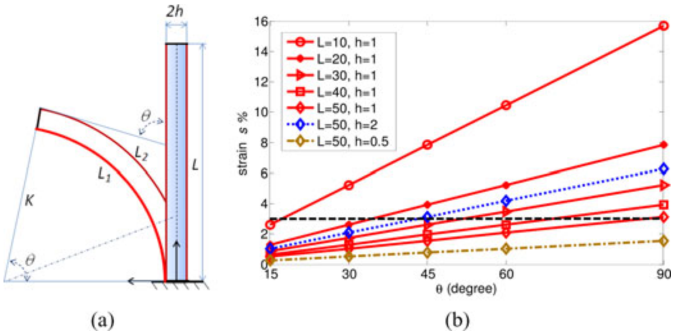

Fig. 9. Structure of the SMA fin ray: (a) flexible plate embedded with two SMA wires (L_1 and L_2), where L denotes the length of the fin ray, h denotes half of the thickness of the flexible plate; and (b) relationship of the deflection angle and strain of SMA wires (the dashed horizontal line denotes 3% strain). Again, θ denotes the angle that the fin ray bends, while s denotes the strain that the SMA wire will contract).

SMA wires to provide a notable deflection angle ($> 60^\circ$) within 3% strain; and 2) decreasing a leads to a larger θ. If $a < 1$ mm and $b = 40$ mm, a larger θ will be produced. However, it is difficult to fix SMA wire on the base part accurately when a is small, as the root of the fin ray is longer than 1 mm and there exists a hinge between the fin ray and the base part; 3) Increasing b leads to a larger θ. However, a large b will cause the difficulty to spread soft membrane on the fin ray.

From the above analysis, a small a or a large b leads to a large deflection angle θ. If a is small enough and b is large enough, the bioinspired fin ray can be designed as a flexible fin ray embedded with SMA wires, as shown in Fig. 9(a). In the figure, SMA wires are closely stuck on the surface of flexible plate. As left SMA wire is heated to A_s, it will contract and pull the flexible plate to bend. The relationship between the bending angle θ and the strain of SMA wire s is calculated and some results are shown in Fig. 9(b). It is observed from the figure: 1) If h is small enough (i.e., implying a small thickness of the plate and a small diameter of SMA wire), the SMA wire will pull the plate to bend with a considerable angle ($L = 50$ mm and $h = 1$ mm/0.5 mm); 2) Bending angle θ is directly proportional to the length of the plate. With the same strain of an SMA wire, a longer plate leads to a larger bending angle.

In summary, the bioinspired fin ray may have a larger bending angle with embedded SMA wires. However, the above analysis is conducted according to the geometrical relationship without performing the force analysis of the SMA fin ray. The actual bending angle of the bioinspired fin ray will be smaller than that from the present analysis because of the drag force from the flexible plate, the unactuated SMA wire, and/or the hydrodynamics.

B. Construction of the SMA-Driven Plate

A flexible plate, embedded with SMA wires and SMA-driven plate, is utilized as the basic unit of the bioinspired pectoral fin. As shown in Fig. 10, the SMA-driven plate consists of a fixed bearing, a flexible base plate, SMA wires, a silica gel membrane, and fixing points. Two SMA wires placed on the top and bottom of the base plate are heated to realize an oscillation. The flexible

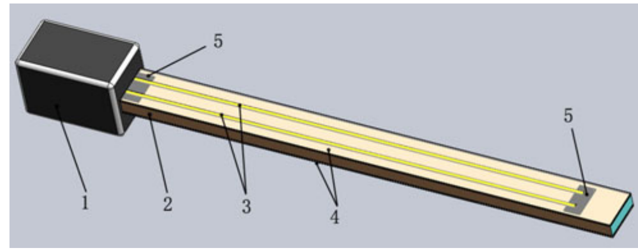

Fig. 10. Structure of the SMA-driven plate. [1) Fixed bearing. 2) Flexible base plate. 3) SMA wires. 4) Silica gel membrane. 5) Fixing points.]

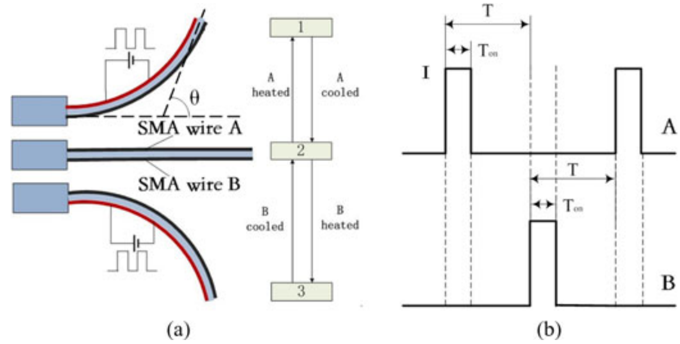

Fig. 11. Oscillation of the SMA-driven plate: (a) control of the bending direction of the SMA-driven plate by heating SWA wires. A and B denote SMA wires on top and bottom surfaces of the plastic plate, respectively. θ denotes the oscillation angle of the SMA-driven plate, which can be measured by the angle between the horizontal line and the tangent to the tip point of the SMA-driven plate; and (b) time sequence of the heating current for SMA wires A and B. $T_{\rm on}$ denotes the duty time in a PWM current, the oscillation frequency of the SMA-driven plate is $1/2T$, T is the phase difference between the heating PWM of SMA wires on two sides of the SMA-driven plate.

plate is made of polyvinyl chloride (PVC) with a high elasticity. The thin membrane, made of silica gel, is adhered to the base plate by glue to protect the SMA wires from the water and keep the wires cling to the base plate while bending. The tip points of SMA are fixed on a small circuit board, which is embedded in the base plate. In order to ensure a relatively large bending angle, the length and the thickness of the SMA-driven plate is set as 50 mm and 1 mm [accordingly to the results shown in Fig. 9(b)], respectively. The width of the SMA-driven plate should match the stress of the SMA wires, which is related to the diameter of the SMA wires. Considering the assembling of SMA wires on the plate, the width of the SMA-driven plate is set as 20 mm. The diameter of the SMA plates will be determined by simulation and experiments.

As illustrated in Fig. 11, as an SMA wire is heated to A_s by passing a pulse width modulation (PWM) current. It will undergo phase transformation, contract to its original length, and pull the tip of the plate. Therefore, the plate will bend to the side where the SMA wire is heated. Since the base plate is flexible, its elastic modulus is large enough to provide a resilience force back to the middle state. When the SMA wire cools, the SMA-driven plate will return straight. By successively heating SMA wires on both sides of the plate with two PWM currents with phase difference, the SMA plate can bend and oscillate.

It is worth mentioning that the motion of the SMA-driven flexible plate is related to the dynamical constitutive equation

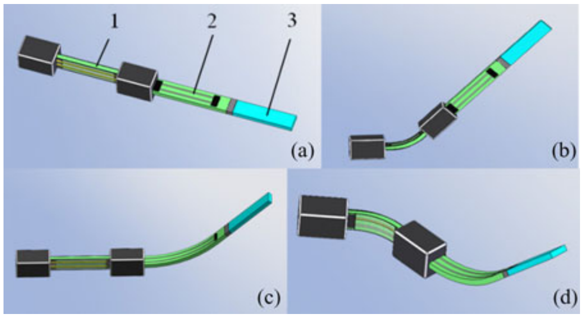

Fig. 12. Structure and state of an SMA fin ray: (1. Root SMA driven plate, 2. Tip SMA driven plate, 3. Elongated plate): (a) Free state. (b) Root SMA-driven plate bending. (c) Tip SMA-driven plate bending. (d) Two SMA plates bending simultaneously.

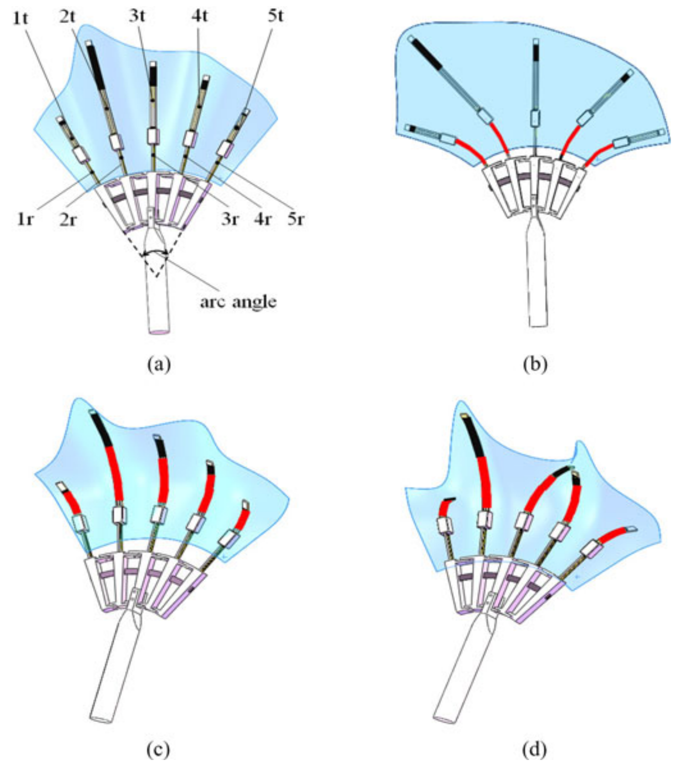

Fig. 13. Illustration of a bioinspired pectoral fin and its four basic patterns: (a) Relaxation: Numbers 1–5 denote the number of five fin rays, "t" stands for tip SMA-driven plates, "r" stands for root SMA-driven plates. (b) Expansion: SMA driven plates 1r, 2r, 4r, and 5r are actuated. (c) Bending: All tip SMA-driven plates are actuated. (d) Undulation: All tip SMA-driven plates are actuated.

of SMA, the thermodynamic between SMA wires and their environment, the dynamics related to large deformation flexible beam, two SMA wires, and hydrodynamics. The dynamics of flexible plates embedded with SMA wires is tedious to model. Therefore, we estimate the diameter of SMA wires through static equilibrium, and determine the range of some key parameters by simulation, such as the diameter of SMA wires and the current that passes through the SMA wires. The details of the SMA-driven plates can then be determined by experiments according to the requirements of a real fin ray, which will be presented in Section IV.

C. Assembly of the Fin Ray by SMA-Driven Plates

Inspired by the motions of fin ray exhibited in Fig. 5, a fin ray can perform two-DoFs motions simultaneously. However, by considering the width of the plate of only 1 mm, it is impossible to assemble another two SMA wires on the flexible plate in its two lateral planes. To imitate the motions of fin rays, two SMA-driven plates are combined serially with their cross sections perpendicular to each other to achieve a 2-D complicate bending motion as shown in Fig. 12. An SMA fin ray is composed of three parts: a root SMA-driven plate, a tip SMA-driven plate, and a flexible elongate plate. The length of all the driven plates is 50 mm, while the length of the elongated flexible plates is varied for different rays.

It should be pointed out that the motion of the bioinspired fin ray is similar to that of a real fin ray in terms of the structural characteristics. The main portion of a real fin ray deforms passively for the hydrodynamic force during motion, whereas a bioinspired fin ray deforms actively for the stress of SMA wires. Despite the difference, the bioinspired pectoral fin is able to produce four basic patterns as will be discussed next.

D. Design of the Bioinspired Pectoral Fin With Multirays

By combining several SMA fin rays, a flexible bioinspired pectoral fin is able to exhibit complex patterns. As the fin rays can bend in two dimensions, the developed flexible bioinspired fin can performs basic patterns extracted in the kinematic experiment. In the bioinspired pectoral fin, the number of SMA fin rays, n, is an important parameter. Based on the kinematic study, undulation is a basic pattern of the pectoral fin, which is also a primary motion in maneuvers. According to the Shannon theorem, in order to imitate an undulation motion, the phase difference $\Delta\varphi$ of two neighboring fin rays should be less than or equal to $\pi/2$. As the relationship between $\Delta\varphi$ and the wave number, n_λ, is $\Delta\varphi = 2\pi n_\lambda/(n-1)$, we have $n \geq 4n_\lambda + 1$. It implies that to achieve a complete wave in an undulation motion, at least five fin rays are needed.

The structure of the bioinspired flexible pectoral fin is shown in Fig. 13. As discussed, five SMA fin rays are adopted and they are placed and assembled radially. A thin membrane covers the five fin rays. The lengths of the five SMA fin rays are different so that the shape of the bioinspired fin is similar to that of a real fish fin [36]. The weight of the whole bioinspired fin is only 150 g, which is considered light for a robotic fish. The key parameters of the bioinspired pectoral fin are listed in Table I.

E. Basic Patterns of the Bioinspired Pectoral Fin

By controlling the SMA-driven plates of each fin ray, we can realize the basic patterns of the bioinspired pectoral fin as shown in Fig. 4. For example, if we bend SMA-driven plates (1r and 2r) in the outside direction and bend SMA-driven plates (4r and 5r) in the opposite direction, the expansion pattern could be achieved as shown in Fig. 13(b). By controlling SMA plates, 1t, 2t, 3t, 4t, and 5t bend in one direction, we can achieve the bending pattern, as shown in Fig. 13(c). To realize the undulation

TABLE I
PARAMETERS FOR THE BIOINSPIRED PECTORAL FIN

Parameters	Specifications
Number of fin rays	5
Surface area (relaxed)	215 cm^2
Weight	150 g
Arc angle	60°
Length of Ray 1	(50+50+10) mm
Length of Ray 2	(50+50+60) mm
Length of Ray 3	(50+50+40) mm
Length of Ray 4	(50+50+20) mm
Length of Ray 5	(50+50+0) mm
Thickness of membrane	0.2 mm
Thickness of flexible plate	1 mm

Note: The length of each ray is the sum of the three connecting parts: the length of root SMA-driven plate, the length of tip SMA-driven plate length, and the length of elongated flexible plate length.

pattern, we control the adjacent fin rays to bend in opposite directions, as shown in Fig. 13(d). Moreover, the undulation motion could be achieved by the successively bending the adjacent SMA plates with a phase difference.

IV. Simulation and Experimental Optimization on SMA-Driven Plates

In the structural design of the robotic pectoral fin, an SMA-driven plate is the most fundamental component of the bioinspired pectoral fin. Its performance greatly affects the movement of the pectoral fin. Different parameters may lead to extremely different response times and oscillation amplitudes. In order to obtain an optimize parameters of the designed SMA-driven plate, a thermodynamic simulation of driving SMA wires is used to investigate the influences of the diameters of SMA wires and the heating current. Experiments of SMA-driven plates oscillating underwater should be conducted to understand the influence of the diameter of SMA wires and the heating current. The result is useful to determine the structural parameters of the SMA-driven plate, which provides a basis for the control of the bioinspired pectoral fin.

A. Characteristics of the SMA-Driven Plate

The SMA-driven plate is composed of three components: SMA actuators, flexible plate, and the membrane. Ni-Ti (50.8%) SMA wires are adopted as the SMA actuators. The Martensitic inverse phase transformation temperature is 55 °C, whereas the Martensitic phase transformation temperature is 27 °C. The elastic modulus of the flexible plate (PVC) is 2.4 GPa.

According to the structure of the SMA-driven plate, a deformable beam model is used. The diameter of the SMA wire is estimated through the static equilibrium of the plate [39]. The simplified force and moment equations of the SMA plate can be stated as

$$A^a E_M \varepsilon_M + AEe + EIK^2 = A^a E_A \varepsilon_A \tag{2}$$

$$(h + d/2)A^a E_M \varepsilon_M + EIK = (h + d/2)A^a E_A \varepsilon_A \tag{3}$$

where ε_M stands for the strain of the SMA wire in martensite phase, and can be expressed as $\varepsilon_M = e + K(h + d/2) + eK(h + d/2)$, in which d stands for the diameter of SMA wires, ε_A stands for the strain of SMA wire in Austenite phase, and it can be expressed as $\varepsilon_A = e - K(h + d/2) - eK(h + d/2) + \varepsilon_{\mathrm{SMA}}$, K is the curvature of the central axis of the plate, and e is the elongation of the flexible plate, these parameters can be easily deduced from the structure shown in Fig. 9(a). Note that E denotes elastic modulus of the flexible plate, while I denotes the moment of inertia of the flexible plate, which is $b(2\ h)^3/12$, in which b and 2 h denote the width and the thickness of the plate, respectively. They are set as 20 and 1 mm as the values suggested in Section III-B. A^a denotes the cross-sectional area of SMA wires, while A denotes the cross-sectional area of the flexible plate. Young's modulus of austenite and martensite, namely E_A and E_M, are 40.8 and 17.5 GPa, respectively.

In order to estimate the diameter of SMA wires, the following assumptions are considered: 1) one SMA wire is totally heated to Austenite phase, while the other one is still in Martensite phase; 2) the strain of the SMA wire $\varepsilon_{\mathrm{SMA}}$ is about 0.03; 3) the SMA-driven plate can bend up to 90°; 4) the mechanical effect of the thin membrane is ignored. With these assumptions, the diameter of the SMA wire (d) is 0.23 mm for the static equilibrium of the SMA plate. The result is useful to the thermodynamics simulation. Note that the estimation is only conducted by the static equilibrium of the plate. Actual motion of the SMA-driven plates is different.

B. Thermodynamic Simulation on the SMA-Driven Plate

A thermodynamic simulation is conducted to evaluate the heating speed and cooling speed of different SMA diameters and heating currents, which is useful to the design of structure and driving strategy. Note that the temperature of SMA is a key factor that affects the motion of the SMA-driven plate, since the shape memory effect is closely linked to temperature.

Several assumptions are made for the thermodynamic simulation: 1) the thermal radiation effects of SMA wires are very small and therefore negligible; 2) the convectional heat between SMA wires and environment is regarded as the only way of heat transformation with a constant heat convectional coefficient h_w; 3) the transformation latent heat of the SMA wires is negligible, since the SMA wire diameter is only about 0.2 mm. The latent heat is also small. Based on these assumptions, the thermodynamic analysis of driving SMA-driven plates underwater is outlined as follows:

1) Heating Process:

$$\int_t \frac{4\rho_e l}{\pi d^2} I^2(t)dt = \int_t \frac{\pi \mathrm{d}^2}{4} \rho c l dT(t) + \int_t h_w \pi dl[T(t) - T_0]dt \tag{4}$$

where electrical conductivity, density, heat capacity, diameter, and length of an SMA wire are characterized by ρ_e, ρ, c, d, and l, respectively. Note that $I(t)$ is the current and T_0 is ambient temperature.

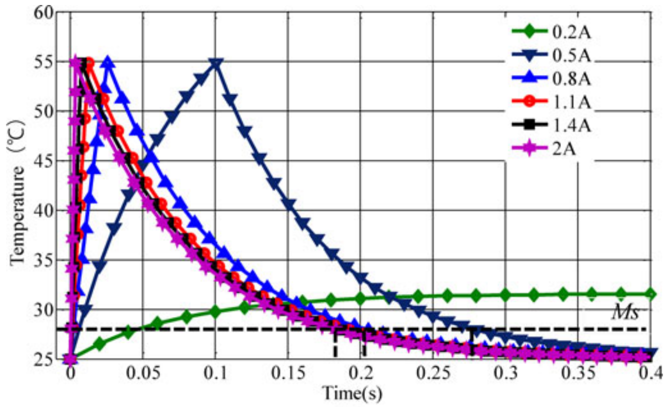

(a)

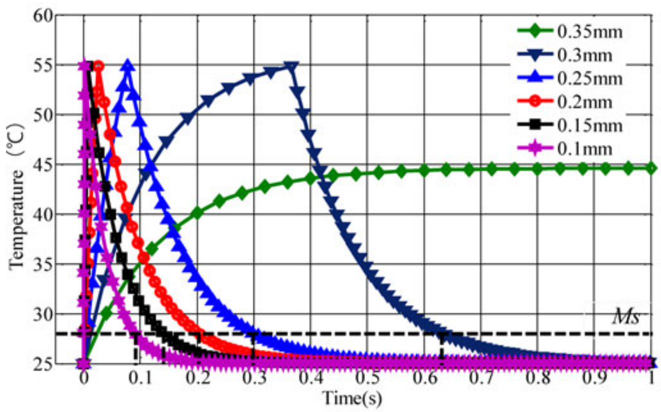

(b)

Fig. 14. Temperature response of the SMA-driven plates (A_s is 55 °C, M_s is 27 °C, h_w is set as 2500 W/m^2 K that is obtained from heating experiments): (a) with respect to different currents, the diameter of the SMA wire is 0.2 mm and (b) with respect to different diameters, the heating current is 0.8 A.

2) Cooling Process:

$$\int_t \frac{\pi \mathrm{d}^2}{4} \rho c l dT(t) + \int_t h_w \pi d l [T(t) - T_0] dt = 0. \qquad (5)$$

Based on (4) and (5), the temperature changes of SMA wires with various parameters can be obtained by virtue of MATLAB simulation. The relationship between temperature and time with different heating currents is shown in Fig. 14(a). According to the estimation in the previous section, the diameter of the SMA wires is set as 0.2 mm. If the heating current is 0.2 A, the SMA wire cannot reach A_s and stays at 31 °C. As for the currents 0.5 and 0.8 A, the heating time is 0.1 and 0.02 s, respectively. When the heating current is higher than 0.8 A, the speed of heating is high and shows insignificant difference. The response frequency of SMA wires can reach a maximum value of up to 6.3 Hz. The influence of diameters of SMA wires is shown in Fig. 14(b). For the heating process, it is seen that as the diameter of the SMA wire is 0.35 mm, the heating current is unable to heat the SMA wire to A_s. This implies that the SMA wire is not able to perform the austenitic transformation and exhibits no output. As for the other five small diameters, the temperature can reach A_s rapidly, in which 0.1 mm shows the fastest speed. For the cooling process, the SMA wires present similar cooling speed since they share the same h_w. By combining the two processes together, we can obtain the response frequency, and for the case of diameter 0.1 mm, the temperature response frequency can reach about 9 Hz.

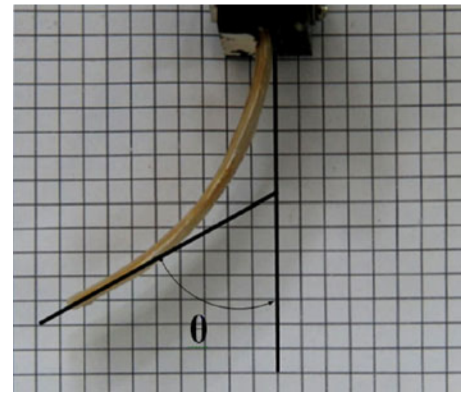

Fig. 15. Illustration of measurement for the oscillation amplitude of the SMA-driven plate.

For an SMA-driven plate, an appropriate SMA wire diameter and the heating current will lead to a high response frequency, which can satisfy the frequency of the kinematic analysis of the live pectoral fin. It is seen from Fig. 14 that, as the heating current is 0.8 A, the SMA wires cannot reach A_s, if the diameter exceed 0.3 mm. For the diameter of 0.2 mm, the heating current 0.2 A could not heat SMA wires to A_S as well. This is a useful finding for the manufacturing and the heating of the SMA-driven plate and provides guidance for the following testing on SMA-driven plates. Based on the above thermodynamic simulation analysis, the SMA diameter (0.1–0.3 mm) and the heating current (0.5–2 A) are chosen for the design and experiments of SMA-driven plate in the study presented in the following section.

C. Underwater Experiments on the SMA-Driven Plate

In order to optimize the SMA profile and to obtain the control of the SMA-driven plates, underwater experiments on the driving of SMA-driven plates is conducted. A high-speed video camera is used to record the oscillation motion of SMA-driven plates. The video images are then processed to obtain the oscillating amplitude of the SMA-driven plate.

As the oscillation amplitude and the frequency are two important parameters used to evaluate the SMA-driven plates, their relationships with respect to the current and the wire diameter are investigated experimentally. The angle θ is defined as the oscillation amplitude of SMA-driven plates, as shown in Fig. 15. The oscillation frequency of SMA-driven plates determined by the heating current is set as 0.5, 1, 2, and 3 Hz, respectively. The experimental results are shown in Fig. 16.

By virtue of Fig. 16, the following findings can be concluded:

1) Usually, the oscillation angle increases as the heating current increases. However, there are several exceptions when the SMA wire diameter is equal to 0.1 mm. The possible reason can be stated below. If the SMA wire diameter is 0.1 mm, its heat capacity is also very low. When a PWM current with a fixed duty time, 100 ms, passes through

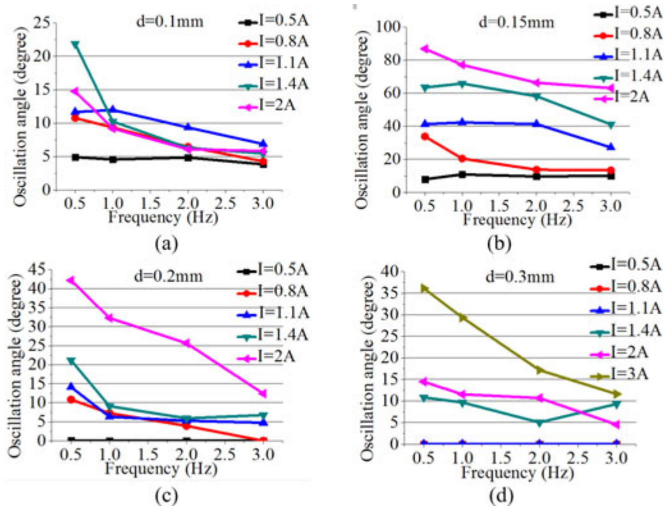

Fig. 16. Oscillation amplitude versus frequency of the SMA-driven plates with various diameters, d. The duty time, T_{on}, of the heating PWM is 100 ms: (a) $d = 0.1$ mm. (b) $d = 0.15$ mm. (c) $d = 0.2$ mm. (d) $d = 0.3$ mm.

the SMA wire, the temperature of the wire will be much higher than A_f, which can also be seen in Fig. 16. Therefore, the SMA temperature cannot decrease under the M_f at the rest time of a heating cycle, 900 ms of 1 Hz, for example. Since the performance of SMA is closely linked to the temperature, this phenomenon greatly affects the deformation rate of SMA, and leads to a rapid decrease of the oscillation angle.

2) As the heating frequency increases, the oscillation amplitude decreases nearly linearly.
3) As the SMA wire diameter is large enough and the heating current is small enough, the SMA-driven plate will keep still, as shown in Fig. 16(c): $I = 0.8$ A and Fig. 16(d): $I =$ 0.5, 0.8, and 1.1 A. The reason is that the temperature of the SMA wire does not reach A_s.
4) The oscillation amplitude of the SMA-driven plate reaches a maximum of 88°, when the SMA wire diameter is 0.15 mm and the frequency is 0.5 Hz.

It can be concluded from Fig. 16 that the predefined oscillation amplitude can be achieved by controlling the heating current and frequency. The performance of the SMA-driven plate with the wire diameter 0.15 mm is found highest, whose oscillation angle ranges from 10° to 88. An experiment with the 5-Hz heating current on the SMA-driven plate is also conducted with 0.15-mm diameter SMA wires. The oscillation amplitude of the SMA-driven plate is still above 5°, which is better than those of other SMA plates driven by the 3-Hz heating current. Note that the oscillation angle here is obtained only by driving SMA plates. It is believed that the oscillation angle of SMA fins will be lower for the hydrodynamics on the SMA fin surface when the SMA plates are equipped. In conclusion, an SMA wire with 0.15-mm diameter is adopted as the driven unit for the bioinspired pectoral fin. The reachable range of changing θ is larger than the range shown in Fig. 7. Even by considering the negative influence of the hydrodynamics on the bioinspired fin, it is still enough for the four basic patterns of a pectoral fin.

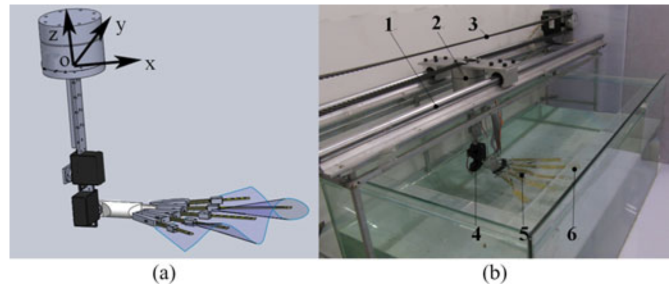

Fig. 17. Experimental setup for force measurement of the bioinspired SMA pectoral fin: (a) Coordination transformation between the force sensor and the bioinspired fin. The force sensor is cylindrical with size 80 mm × 60 mm (diameter × height), the measurement range: $F_x = 125$ N, $F_y = 125$ N, $F_z =$ 125 N, $M_x = 5$ Nm, $M_y = 5$ Nm, $M_z = 10$ Nm, the comprehensive accuracy: $\leq$0.8% FS, resolution: $\leq$0.1% FS, allowable overload: $\leq$150% FS, and data processing cycle: $\leq$1 ms; and (b) Experimental setup, which includes: 1. Linear guide system. 2. Six dimensional force sensor. 3. Synchronization transmission system. 4. Flapping and pitching device. 5. Bio-inspired SMA pectoral fin. 6. Tank, the size of tank is 50 cm × 45 cm × 40 cm.

According to the simulation result presented in the previous section, the oscillation frequency of the SMA-driven plate is 7 Hz, which is similar to the value obtained in the experiment, 5 Hz. The difference between the frequency obtained from the simulation and the experiment arises from the hypothesis that some energy loss is omitted and the coefficient h_w is set as a constant in simulation.

V. Experiments on the Bioinspired Pectoral Fin

During the swimming process, pectoral fins of fish provide propulsion to maintain balance and maneuverability as a result of hydrodynamic interaction between the pectoral fins and water. In order to study the motions of the bioinspired flexible SMA pectoral fin, we carried out the experiments in executing three motions: expansion, flapping, and undulation (arising from the basic patterns shown in Figs. 4 and 13, respectively). The experiment setup is shown in Fig. 17. A 6-D force sensor is installed above the bioinspired pectoral fin. The sensor is used to measure the three-orthogonal-direction forces (F_x, F_y, F_z) and three-orthogonal-direction torques (M_x, M_y, M_z) generated by the motion of the bioinspired pectoral fin. Note that the lateral force, thrust force, and lift force that are generated by the SMA fin are represented by F_x, F_y, and F_z, respectively.

A. Expanding Motion of the Bioinspired Pectoral Fin

Expanding motion changes the fin surface area and leads to changes in hydrodynamics forces. Its actuating mechanism is displayed in Fig. 13(b), while the biorobotic fin expanding motion is shown in Fig. 18. As mentioned in Section II-C, the expansion coefficient β (=S/S$_0$) is used to evaluate the area change of a pectoral fin. The area is calculated by counting the grids covered by the robotic fin. The effect of the heating current and heating time is also investigated. The relationship between the expansion coefficient and the heating current in a bioinspired flexible pectoral fin expansion is shown in Fig. 19. The following conclusion can be drawn by virtue of the figure.

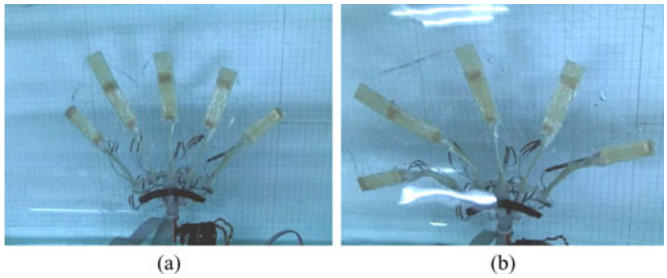

Fig. 18. Expansion motion of the biorobotic pectoral fin. (a) Relaxation. (b) Expansion.

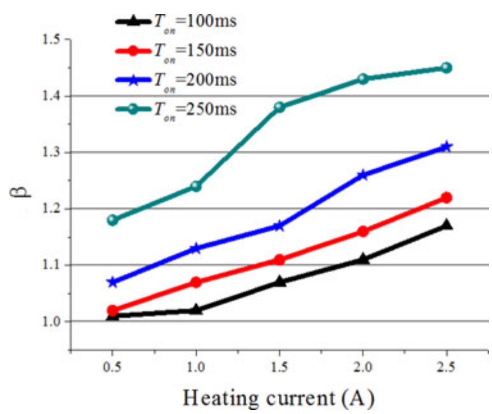

Fig. 19. Relationship between expansion degree, the current, and duty time in the bioinspired pectoral fin expansion experiment.

1) For a specific duty time T_{on}, β increases as the heating current increases. For T_{on} with the value of 100, 150, and 200 ms, the increasing gradient is the same. As for a T_{on} with 250 ms, the increasing speed of β slows down when the heating current is higher than 1.5 A. And it seems to reach the saturated expansion degree when the heating current is 2.5 A.
2) For a fixed heating current, β also increases with T_{on}. The maximum value of β is 1.45, where S_0 equals to 215 cm^2 and S equals 312 cm^2.

The experimental result suggests that the bioinspired pectoral fin could expand in a considerable degree. It can fulfill the requirement obtained from the kinematic study of the real pectoral fin (as shown in Fig. 5) with the maximum expansion coefficient of 1.4. It seems to imply that any β within this range can be obtained by simply alternating the heating current and T_{on}.

B. Bending Motion of the Bioinspired Pectoral Fin

According to the analysis in Section III, by bending the tip SMA-driven plate in one direction simultaneously, the biorobotic fin can realize a required bending motion [see Fig. 13(c)]. An experiment was conducted to explore the bending motion of the biorobotic pectoral fin. In the experiment, the heating frequency is 2 Hz, which is similar to the result of the kinematic study on the Koi Carp. The duty time T_{on} is 150 ms, which implies that the bending stage is taken as 150 ms, while

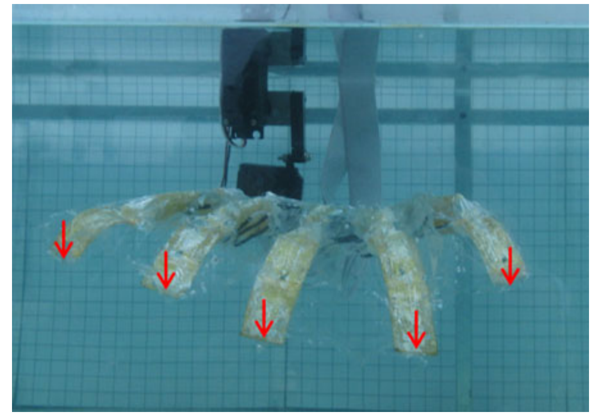

Fig. 20. Snapshot of the flapping motion by the biorobotic pectoral fin.

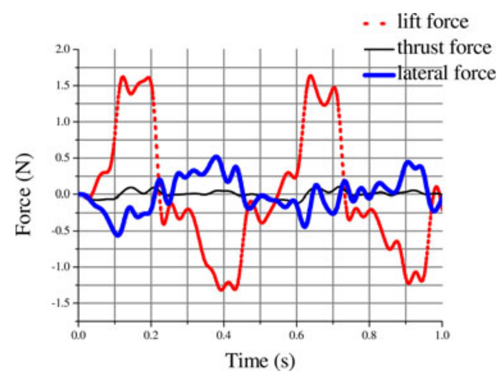

Fig. 21. Force in the bending motion of the bioinspired pectoral fin. The heating frequency is 2 Hz, where $T_{\mathrm{on}} = 150$ ms, $I = 1$ A.

the recovery stage takes 350 ms. The hydrodynamics forces are also measured and investigated in the experiment. Fig. 20 shows a snapshot of the flapping motion of the biorobotic pectoral fin.

The lift force, thrust force, and lateral force of the pectoral fin are obtained and shown in Fig. 21.

In the bending stage, the lift force peak reaches 1.6 N, while in the recovery stage, the force peak reaches 1.3 N with an average value of positive 0.35 N. The lateral force has a peak of 0.5 N, while the thrust force is less than 0.1 N. Among the three forces, the lift force can reach the largest peak, three times of the lateral force, whereas the thrust force is very small if compared with the other two forces. It demonstrates that the bioinspired pectoral fin can generate a dominate force along the bending direction by the bending motion. This is the similar finding observed from the kinematic movement depicted in Fig. 2. The flapping motion is a major motion in fish retreating. The dominated bending directing force will generate a direct drag force to retreat the body. The other two forces, which are not the major forces of the bending motion, are used for balancing body when maneuvering. Note that the main part of the bioinspired fin deforms actively for SMA actuating, while that of the live fish fin deforms passively for the hydrodynamics during fin flapping. The phase of the force might be different for the same morphology of the fins.

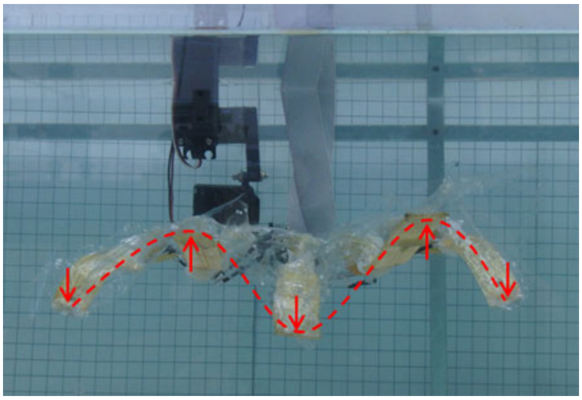

Fig. 22. Snapshot of the undulation motion by the biorobotic pectoral fin.

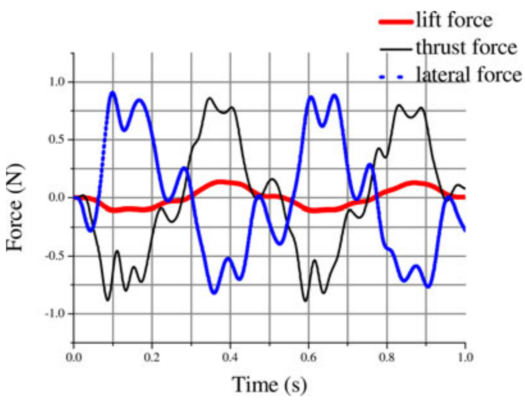

Fig. 23. Force components in the undulation motion of the bioinspired pectoral fin of two periods. The heating frequency is 2 Hz, $T_{\rm on} = 150$ ms, $I = 1$ A.

C. Undulation Motion of the Bioinspired Pectoral Fin

An undulation motion of the bioinspired pectoral fin is obtained by driving the five SMA-driven plates intermittently as shown in Fig. 13(d). A snapshot of the undulation of the bioinspired pectoral fin is shown in Fig. 22.

The hydrodynamic forces are also investigated and presented in Fig. 23. It is seen that the lateral force is the largest with the peak value 0.9 N and the average value is 0.15 N. The thrust force has the similar magnitude to the lateral force with an average value of 0.11 N, while the lift force is relatively small in this motion. The reason could be that the fin rays are placed radially. Also, the forces generated in undulation are mainly distributed over the horizontal plane. By corresponding to the real fish movements and by considering the fact that the pectoral fin seems to be almost perpendicular to the fish body in the hovering cycle, the undulation motion mainly generates a lift force to overcome gravity and a lateral force to avoid yawing by the cooperation of two pectoral fins.

D. Discussion

Several researchers have also conducted studies on hydrodynamic forces of robotic pectoral fins in different motions. Lauder *et al.* [11] developed a robotic pectoral fin and achieved expansion, curling, and cupping motions with five fin rays varying from 9 to 12.5 cm. By measuring the thrust force of cup, sweep, and their combination motion, they found that the cup and sweep motion can generate a considerably higher thrust force as well as a small drag force with a peak force of 0.2 N. On the other hand, Tangorra *et al.* [18] developed a robotic pectoral fin with five fin rays varying from 8.5 to 13.5 cm. They analyzed the thrust force of sweep, curl, expansion, cupping, and the combination motion and the maximum peak thrust force reaches 0.6 N. The trend of their results is the same as that of the results presented in this paper.

VI. Concluding Remarks

This paper is concerned with a detailed design and initial experiments of a bioinspired flexible SMA pectoral fin. The kinematic observation of the pectoral fin of a Koi Carp has been presented. Several basic patterns of the pectoral fin are first obtained by analyzing the fin motions captured by videos. On the other hand, an SMA fin ray capable of two-DoFs oscillation is introduced and a lightweight bioinspired pectoral fin formed by the SMA fin rays is developed. For the detailed design, the simulation and experiment on the SMA-driven plate have been conducted. The results demonstrate the validity of the proposed SMA-based mechanism, in terms of the motion generation, lightweight, and ease of assembly.

The biological pectoral fin exhibits several complex motions analyzed in Section II. The motions of the pectoral fin arise from the four basic patterns that are extracted by digital image processing from the movement of pectoral fins in fish hovering and retreating. The result is similar to that obtained in the study on the pectoral fin of the sunfish [11], [18]. Tangorra *et al.* [18] investigated various motions of the sunfish pectoral fins. The curl and expansion in their study have similar features to our SMA pectoral fin. On the other hand, cupping, which is not presented here, is actuated by the dorsal leading ray and ventral leading ray. Two aspects of patterns combination, space and time, should be considered in future for the implementation of more complex motions. The space-time combination implies that two or more patterns exhibit simultaneously, for example, expanding and bending. The time combination is concerned with switching patterns along with time, for example, from flapping to undulation. For these problems with multiple variables, the parametric study used in [40] is worth considering for the comprehensive analysis and computation.

The proposed bioinspired pectoral fin possesses several major features as those by the biological fin. For example, the fin could provide the motion with four basic patterns: relaxation, expanding, bending, and undulation. It is obvious that the bioinspired pectoral fin is still a very simplified version of the biological pectoral fin. A live pectoral fin of a Koi Carp has 15 fin rays [36], whereas only five fin rays are used in the bio-inspired fin developed here. More fin rays require more DoFs and are therefore more tedious in the implementation and control of fin motion. It will be useful to investigate the optimal number of fin rays to provide the "natural" motion required in the maneuver. The model presented here should be extended to the motion control of the bioinspired fish actuated by multiple joints (or different types of fins) [17]. For flexible fins with significant length, a beam model with various boundary conditions might be useful in the modeling of the fin motion [41].

It is worth emphasizing that the purpose of the bioinspired fin is not to replicate fully the morphology of the Koi Carp pectoral fin or not to perform exactly as that of the live pectoral fin. The desired bioinspired pectoral fin capable of various key patterns should be developed to provide the maneuvers of a robotic fish. The bioinspired fin should be relatively simple and lightweight. The propulsion of SMA-driven fins should be able to enhance the stability and maneuverability of robots. Furthermore, one should explore some new motions with the bioinspired fin that emerge from other motions of the fish, such as steady swimming and gliding, or even new motions that do not execute live fins, but useful to the maneuvering of the fish robots.

ACKNOWLEDGMENT

The authors would like to thank the reviewers for their constructive comments, which have greatly improved the quality of the revised manuscript.

REFERENCES

[1] M. S. Triantafyllou, G. S. Triantafyllou, and D. K. P. Yue, "Hydrodynamics of fish swimming," *Annu. Rec. Fluid Mech.*, vol. 32, pp. 33–53, 2000.
[2] M. Sfakiotakis, D. M. Lane, and J. B. C. Davies, "Review of fish swimming modes for aquatic locomotion," *IEEE J. Ocean. Eng.*, vol. 24, no. 2, pp. 237–252, Apr. 1999.
[3] G. V. Lauder and E. G. Drucker, "Morphology and experimental hydrodynamics of fish fin control surfaces," *IEEE J. Ocean. Eng.*, vol. 29, no. 3, pp. 556–571, Jul. 2004.
[4] P. W. Webb, "Stability and maneuverability," *Fish Biomech.*, vol. 23, pp. 281–332, 2005.
[5] M. W. Westneat, "Functional morphology of aquatic flight in fishes: Kinematics, electromyography, and mechanical modeling of labriform locomotion," *Amer. Zool.*, vol. 36, pp. 582–598, 1996.
[6] M. Westneat, D. H. Thorsen, J. A. Walker, and M. Hale, "Structure, function, and neural control of pectoral fins in fishes," *IEEE J. Ocean. Eng.*, vol. 29, no. 3, pp. 674–683, Jul. 2004.
[7] D. H. Thorsen and M. W. Westneat, "Diversity of pectoral fin structure and function in fishes with labriform propulsion," *J. Morphol.*, vol. 263, pp. 133–150, 2005.
[8] L. J. Rosenberger, "Functional morphology of undelatory pectoral fin locomotion in the stingray Taeniura lymma (chondrichthyes: dasyatidae)," *J. Exp. Biol.*, vol. 202, pp. 3523–3539, 1999.
[9] L. J. Rosenberger, "Pectoral fin locomotion in batoid fishes: Undulation versus oscillation," *J. Exp. Biol.*, vol. 204, pp. 379–394, 2001.
[10] G. V. Lauder, P. Madden, R. Mittal, H. Dong, and M. Bozkurttas, "Locomotion with flexible propulsors: I. Experimental analysis of pectoral fin swimming in sunfish," *Bioinsp. Biomim.*, vol. 1, pp. s25–s34, 2006.
[11] G. V. Lauder, E. J. Anderson, J. Tangorra, and P. G. A. Madden, "Fish biorobotics: Kinematics and hydrodynamics of self-propulsion," *J. Exp. Biol.*, vol. 210, pp. 2767–2780, 2007.
[12] G. V. Lauder, P. G. A. Madden, J. L. Tangorra, W Anderson, and T. V. Baker, "Bioinspiration from fish for smart material design and function," *Smart Mater. Struct.*, vol. 20, no. 9, pp. 094014-1–094014-13, 2011.
[13] P. E. Sitorus, Y. Y. Nazaruddin, E. Leksono, and A. Budiyono, "Design and implementation of paired pectoral fins locomotion of labriform fish applied to a fish robot," *J. Bionic Eng.*, vol. 6, no. 1, pp. 37–45, 2009.
[14] S. Yang, J. Qiu, and X. Han, "Kinematics modeling and experiments of pectoral oscillation propulsion robotic fish," *J. Bionic Eng.*, vol. 6, no. 2, pp. 174–179, 2009.
[15] K. H. Low and A. Willy, "Biomimetic motion planning of an undulating robotic fish fin," *J. Vib. Control*, vol. 12, no. 12, pp. 1337–1359, 2006.
[16] K. H. Low, "Modeling and parametric study of modular undulating fin rays for fish robots," *Mech. Mach. Theory*, vol. 44, pp. 615–632, 2009.
[17] C. Zhou and K. H. Low, "Design and locomotion control of a biomimetic underwater vehicle with fin propulsion," *IEEE/ASME Trans. Mechatronics*, vol. 17, no. 1, pp. 25–35, Feb. 2012.
[18] J. L. Tangorra, S. N. Davidson, I. W. Hunter, P. G. A. Madden, G. V. Lauer, H. Dong, M. Bozkurttas, and R. Mittal, "The development of a biologically inspired propulsor for unmanned underwater vehicles," *IEEE J. Ocean. Eng.*, vol. 32, no. 3, pp. 533–550, Jul. 2007.
[19] J. L. Tangorra, G. V. Lauder, I. W. Hunter, R. Mittal, P. Madden, and M. Bozkurttas, "The effect of fin ray flexural rigidity on the propulsive forces generated by a biorobotic fish pectoral fin," *J. Exp. Biol.*, vol. 213, pp. 4043–4054, 2010.
[20] J. Tangorra, C. Phelan, C. Esposito, and G. Lauder, "Use of biorobotic models of highly deformable fins for studying the mechanics and control of fin forces in fishes," *Integr. Comp. Biol.*, vol. 51, pp. 176–189, 2011.
[21] S. Guo, T. Fukuda, and K. Asaka, "A new type of fish-like underwater microrobot," *IEEE/ASME Trans. Mechatronics*, vol. 8, no. 1, pp. 136–141, Mar. 2003.
[22] A. Suleman and C. Crawford, "Design and testing of a biomimetic tuna using shape memory alloy induced propulsion," *Comput. Struct.*, vol. 86, pp. 491–499, 2008.
[23] J. Finkbeiner, J. Ahmad, W. Santosa, G. Xu, and J. Xiao, "Biomimetic fish actuated by shape memory alloy," in *Proc. IEEE Conf. Ind. Electron. Appl.*, Jun. 2011, pp. 2139–2144.
[24] A. Villanueva, C. Smith, and S. Priya, "A biomimetic robotic jellyfish (robojelly) actuated by shape memory alloy composite actuators," *Bioinsp. Biomim.*, vol. 6, pp. 36004-1–36004-16, 2011.
[25] M. Aureli, V. Kopman, and M. Porfiri, "Free-locomotion of underwater vehicles actuated by ionic polymer metal composites," *IEEE/ASME Trans. Mechatronics*, vol. 15, no. 4, pp. 603–614, Aug. 2010.
[26] Y. Fang, T. J. Pence, and X. Tan, "Fiber-directed conjugated polymer torsional actuator: Nonlinear elasticity modeling and experimental validation," *IEEE/ASME Trans. Mechatronics*, vol. 16, no. 4, pp. 656–664, Aug. 2011.
[27] T. Ganley, D. L. S. Hung, G. Zhu, and X. Tan, "Modeling and inverse compensation of temperature-dependent ionic polymer-metal composite sensor dynamics," *IEEE/ASME Trans. Mechatronics*, vol. 16, no. 1, pp. 80–89, Feb. 2011.
[28] Z. Chen, S. Shatara, and X. Tan, "Modeling of biomimetic robotic fish propelled by an ionic polymer-metal composite caudal fin," *IEEE/ASME Trans. Mechatronics*, vol. 15, no. 3, pp. 448–459, Jun. 2010.
[29] Z. Wang, G. Hang, Y. Wang, J. Li, and W. Du, "Embedded SMA wire actuated biomimetic fin: A module for biomimetic underwater propulsion," *Smart Mater. Struct.*, vol. 17, pp. 25039-1–25039-11, 2008.
[30] Z. Wang, G. Hang, J. Li, Y. Wang, and K. Xiao, "A micro-robot fish with embedded SMA wire actuated flexible biomimetic fin," *Sens. Actuators A, Phys.*, vol. 144, pp. 354–360, 2008.
[31] S. Seok, C. D. Onal, K.-J. Cho, R. J. Wood, D. Rus, and S. Kim, "Meshworm: A peristaltic soft robot with antagonistic nickel titanium coil actuators," *IEEE/ASME Trans. Mechatronics*, vol. 18, no. 5, pp. 1485–1497, Oct. 2013.
[32] J.-S. Koh and K.-J. Cho, "Omega-shaped inchworm-inspired crawling robot with large-index-and-pitch (LIP) SMA spring actuators," *IEEE/ASME Trans. Mechatronics*, vol. 18, no. 2, pp. 419–429, Apr. 2013.
[33] C. D. Onal, R. J. Wood, and D. Rus, "An origami-inspired approach to worm robots," *IEEE/ASME Trans. Mechatronics*, vol. 18, no. 2, pp. 430–438, Apr. 2013.
[34] Q. Yan, W. Wu, S. Zhang, M. Xu, and J. Yang, "Preliminary study of flexible pectoral fin capable of 3D motions actuated by shape memory alloy," in *Proc. IEEE Int. Conf. Robot. Biomimetics*, Guilin, China, 2009, pp. 1814–1819.
[35] Q. Yan, S. Zhang, and J. Yang, "Initial implementation of basic actuated unit of a flexible pectoral fin driven by SMA," in *Proc. IEEE Int. Conf. Mechatronics Autom.*, Xi'an, China, 2010, pp. 899–904.
[36] Q. Yan, L. Wang, B. Liu, J. Yang, and S. Zhang, "A novel implementation of a flexible robotic fin actuated by shape memory alloy," *J. Bionic Eng.*, vol. 9, no. 2, pp. 156–165, 2012.
[37] L. Wang, M. Xu, B. Liu, K. H. Low, J. Yang, and S. Zhang, "A three-dimensional kinematics analysis of the Koi Carp pectoral fin by digital image processing," *J. Bionic Eng.*, vol. 10, no. 2, pp. 210–221, 2013.
[38] S. Alben, P. G. Madden, and G. V. Lauder, "The mechanics of active fin-shape control in ray-finned fishes," *J. R. Soc. Interface*, vol. 4, pp. 243–256, 2007.
[39] B. J. Blonk and D. C. Lagoudas, "Actuation of elastomeric rods with embedded two-way shape memory alloy actuators," *Smart Mater. Struct.*, vol. 7, pp. 771–783, 1998.
[40] K. H. Low and C. W. Chong, "Parametric study of the swimming performance of a fish robot propelled by a flexible caudal fin," *Bioinsp. Biomim.*, vol. 5, no. 4, p. 046002, 2010.

[41] K. H. Low, "A comprehensive approach for the eigenproblem of beams with arbitrary boundary-conditions," *Comp. Struct.*, vol. 39, no. 6, pp. 671–678, 1991.

Shiwu Zhang received the B.S. degree in mechanical and electrical engineering and the Ph.D. degree in precision instrumentation and precision machinery from the University of Science and Technology of China (USTC), Hefei, China.

He is currently an Associate Professor in the Department of Precision Machinery and Precision Instrumentation, USTC. He has also been a Postdoctoral Research Fellow in the Department of Computer Science, Hong Kong Baptist University, Hong Kong. He has led a number of research programs sponsored by the National Science Foundation of China, Chinese Academy of Sciences, Chinese State High-Tech Development Plan, Chinese Aeronautical Foundation, etc. He has authored or coauthored more than 50 technical peer-reviewed papers. His current research interests include smart materials and their applications in bioinspired robots, amphibious robots, and terradynamics that involves interactions between locomotion mechanisms and sandy or muddy substrates.

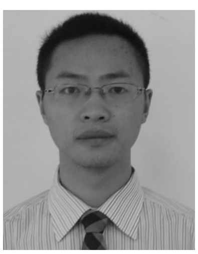

Bo Liu was born in Nanchong, China, in 1988. He received the B.Eng. degree in mechanical engineering from the University of Science and Technology of China, Hefei, China, in 2010, where he is currently working toward the Ph.D. degree.

His research interests include pectoral fin design and numerical simulation, including computational fluid dynamics and fluid-structure interactions.

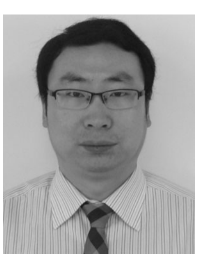

Lei Wang was born in Anqing, China, in 1987. He received the Bachelor's degree in test and control technology and instruments from Hefei University of Technology, Hefei, China, in 2009. He is currently working toward the Ph.D. degree in precision instruments and machinery at the University of Science and Technology of China, Hefei.

His current research interests include bionic robots and digital image processing.

Qin Yan was born in Nanning, China, in 1983. He received the Ph.D. degree in precision instrumentation and precision machinery from the University of Science and Technology of China, Hefei, China, in 2011.

He is currently a Research Assistant in the Department of Machinery and Electric, Suzhou University of Science and Technology, Suzhou, China. His research interests include smart materials and biomimetic devices.

Kin Huat Low received the B.Sc. degree from National Cheng Kung University, Tainan City, Taiwan, and the M.Sc. and Ph.D. degrees in mechanical engineering from the University of Waterloo, Waterloo, ON, Canada.

He is currently a Professor in the School of Mechanical and Aerospace Engineering, Nanyang Technological University, Singapore. His teaching and research interests include robotics, vibrations, impacts, exoskeleton systems, mechatronics design, machines, and mechanisms. He is an author or coauthor of about 250 journal and conference papers in the areas of biomimetics, robotics, rehabilitation, impacts, machine and mechanisms design, power transmission systems, structural dynamics, and vibrations.

Dr. Low won the best paper awards/finalists at several IEEE international conferences for his work on biomimetics, exoskeletons, and rehabilitation. He has also been invited as a keynote speaker in the areas of robotics gait rehabilitation and bioinspired underwater robotics. As for professional services, he has contributed to several journals as an Associate Editor, including *Mechanism and Machine Theory*, *Journal of Bionic Engineering*, IEEE TRANSACTIONS ON AUTOMATION SCIENCE AND ENGINEERING, *Journal of Robotics*, and *Mechatronics*. He has also been the Guest Editor of several journal special issues on bioinspired systems and robotics rehabilitation. He is currently serving as the Chair of the Technical Committee on Biorobotics.

Jie Yang received the Graduate degree from the Department of Physical Chemistry, Beijing University of Science and Technology, Beijing, China, in 1969.

He is currently a Professor in the Department of Precision Machinery and Precision Instrumentation, University of Science and Technology of China, Hefei, China. He leads several research groups focusing on intelligent robots supported by the National Science Foundation of China and the 863 Project. His research interests include intelligent robots, precision machinery materials, and high-speed photography.